ISSN 1087-6596, Glass Physics and Chemistry, 2021, Vol. 47, Suppl. 1, pp. S10–S20. © Pleiades Publishing, Ltd., 2021.

Radiation Shielding Properties for $NaO-CdO-Bi_2O_3-B_2O_3$ Glasses Using XCOM, Phy-X/PSD and Srim Programs

Y. S. Alajerami[a, b, *]

[a] *Faculty of Applied Medical Sciences, Al Azhar University-Gaza, Palestine*

[b] *Department of Physics and Astronomy, Ohio University, Athens, OH, 45701 USA*

**e-mail: yasser_ajr@hotmail.com*

Received December 16, 2021; revised February 1, 2022; accepted February 8, 2022

Abstract—Achieving an excellent and efficient radiation shielding for various applications is impervious. A series of glass samples $20Na_2O{\cdot}15CdO{\cdot}xBi_2O_3{\cdot}(65-x)B_2O_3$ where (x = 0, 10, 20 and 30) were fabricated by the traditional melt-quench method. The structural, chemical stability and significant mechanical properties were explored. The obtained results revealed that the addition of Bi_2O_3 to the glass context enhances the density and reduce values of Poisson ratio (σ). Comprehensive shielding properties for gamma, neutron, proton and alpha ray were estimated by using XCOM, Phy-X/PSD and SRIM programs. MCNP (version 5) has been used to simulate the mass attenuation coefficient (μ/ρ) at different energies (0.1, 0.5, 1, 3, 5 and 15 MeV). A consistent behavior reported with XCOM and Phy-X. The addition of Bi_2O_3 showed significant enhancement in μ/ρ values. In contrast, the addition of Bi_2O_3 in the cost of B_2O_3 leads to a gradual reduction in the values of the projected range and Mass Stopping Power (MSP) for alpha and proton, and the same behavior can be noted for the effective removal cross-section of fast neutron (Σ_R) values. Finally, the new glass composition can be valuable for ionizing radiation shielding applications.

Keywords: bismuth borate glass, SRIM, radiation shielding

DOI: 10.1134/S1087659621070026

INTRODUCTION

Understandable and fast developments in technological and communications sectors in recent years, which led human beings to expose to various types of ionizing radiation such as gamma, neutron radiation and X-ray used in industries, medical and research for varies purposes. The radiation shielding is one of the protective measures to reduce hazards of radiation exposure through avoiding the direct interaction with biological tissues. The hazard of radiation progressively increase by increasing radiation penetration power. The degree of penetration depends mainly on the type and energy of radiation involved, thus the studies made in different type of materials for shielding purposes. Radiation shielding materials for radiation attenuation should have high density, good radiation attenuation, high stability and low toxicity in manufacture process. The effeciency of shielding materials with better radiation shielding resistivity is depends on few factors such as cost, quality, thermal and optical properties, mechanical stability, toxicity and efficacy of attenuation [1–7].

For long time, lead is used as the best material for radiation shielding because of its high atomic number, economical evaluable, available in different form and cheap. However, lead is heavy in weight, easy to crack and somewhere harmful to human health and the environment. Also, concrete shielding materials are becoming more widespread at the different fields of high-energy and nuclear radiations protection. Nevertheless, concretes are opaque and blocking visible light. Therefore, major challenges occur since it is hard to look through the concretes based shield during the control mechanism [8–10].

The glass is highly flexiable for chemical and structural changes by adding modifiers to meet specific applications requirements. However, a typical glass can be defined as transparent, non-toxic and useable with advanced material characteristics for different aims. Hence, researchers desired use glasses as shielding materials in recent applications as they have good capability physically and chemically. Glass has good light transparency, ease of manufacture, non-toxic and high density. Furthermore, glasses can be prepared in the desired shape with high space homogeneity and low costing [11–14].

From the several glass formers, boron oxides (B_2O_3) are the most effecient and important commercial glass. These oxides have attractive properties such as high transmittance, low melting point, thermal and mechanical stability. Bi_2O_3 is highly unstable due to presence of ion pairs, which make these glasses to

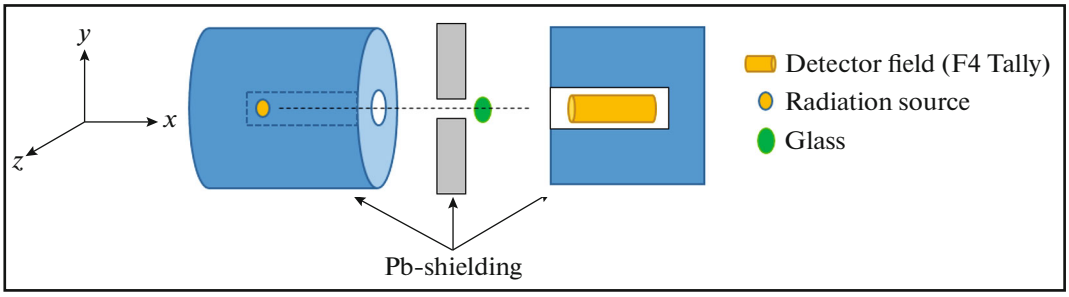

Fig. 1. Total simulation geometry using MCNP5.

exhibit non-liner optical effects. High third order nonlinear optical susceptibility and long infrared cutoff wavelengths make them useful for ultra-fast optical switches and optoelectronic devices. Previous studies proved that the increment of Bi_2O_3 content increase the number of non-bridging oxygen decreased melting temperature to 980°C and decrease coordination number of boron [15–21]. The current study focuses mainly on providing new glasses for gamma ray and neutron shielding applications. It aims to explore the effect of increasing various amounts of Bi_2O_3 in altering structural and shielding properties of borate glass network.

EXPERIMENTAL

Glass Preparation

The current raw materials (Na_2O, CdO, Bi_2O_3 and B_2O_3) are obtained from Alfa Aesar with high purity (99.5% and above). The melting-quenching technique was performed to fabricate the new glasses. Various melting temperatures are performed depend on the Bi_2O_3 concentration (800 to 900°C). finally, the samples shifted to the annealing furnace (temperature 400°C) for 3 h then brought down the temperature to the room temperature during 24 h. The glass systems were prepared based on the stoichiometry:

S1: 20Na_2O, 15CdO and 65B_2O_3 (mol %)

S2: 20Na_2O, 15CdO, 10Bi_2O_3 and 55B_2O_3 (mol %)

S3: 20Na_2O, 15CdO, 20Bi_2O_3 and 45B_2O_3 (mol %)

S4: 20Na_2O, 15CdO, 30Bi_2O_3 and 35B_2O_3 (mol %).

Shielding Properties

In this study, the mass attenuation coefficients of the new samples were estimated by using different methods MCNP5, Phy-X and XCOM programs. A series of gamma shielding properties such as buildup factor (exposure and absorption), electron density (electron/m^3), specific gamma ray constant factor (Rm^2/Ci.h) and gamma dose rate (R/h) were determined by using Phy-X [22].

The shielding parameters of neutron beam were also identified and compared with the available shielding materials by determining the fast removal cross-section (cm^{-1}), and compared with that measured by Phy-X.

In addition, the mass stopping power and projected range of proton and alpha particles were estimated by using SRIM code [23, 24]. This code is a Monte Carlo simulation base that used to estimate the stopping power of ions in materials. The interaction of heavy charged particles (proton/alpha) in a specific material determined based on the Beth-Bloch theorem [23].

MCNP5 Simulation and Interaction Code

Concerning the simulation part, the mass attenuation coefficient of the new samples were estimated by using MCNP5 [25–27]. Figure 1 exhibits the simulation conducted to estimate attenuation coefficients of the prepared glasses. In the x-axis direction, a simple sphere of glass was exposed with a mono-energetic beam emission, which supposed as a conventional point source. Mesh tally type F4 was activated to estimate the sum of all contributions in the proposed detecting area (NaI-detector). To eliminate effect of background radiation, all irradiation process starting from the source to the detector guided and collimated with Pb-shielding. The simulation was conducted by using the weight fractions obtained from the glass compositions. All required data card and commands such as energy (ERG), type of particle (PAR), position (POS) and beam direction (DIR) were defined accordingly. To reduce errors and variance of variance, the simulation was simplified, repeated three times for each glass sample, termination steps applied after high number of histories (NPS > 10^8) and CUT-OFF option was used to exclude low radiation exposure (<1 keV).

RESULTS AND DISCUSSION

Amorphous Phase and Physical Measurments

Figure 2 shows the X-ray powder diffraction (XRD) of the prepared samples. No sharp diffraction peak reported between 20° and 80° theta angle in all tested samples. Instead, broad peaks at 28° and 47° were clearly shown with the new fabricated samples.

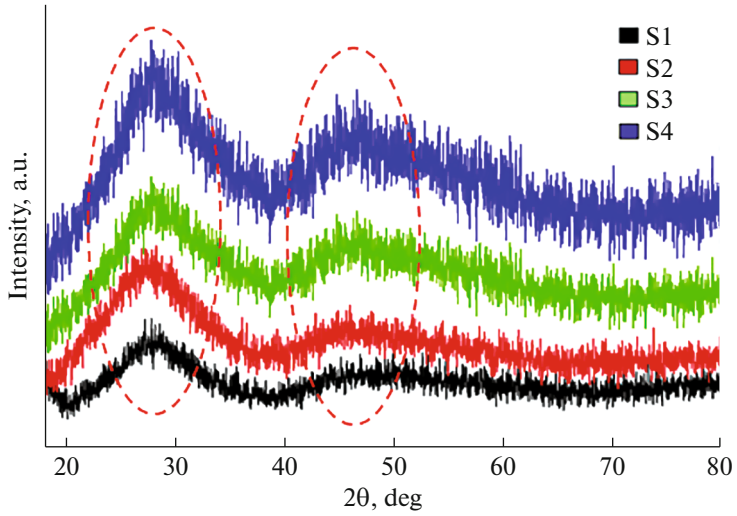

Fig. 2. XRD spectra of the prepared samples.

The spectra obtained from the measurements confirm the amorphous nature of the samples.

Glass Durability

The dissolution rate (*Dr*) of the fabricated glasses was estimated by using the formulae (1) [28]:

$$Dr = \Delta w/At,$$

where, Δw is the weight loss during the immersion, A is the surface area of the fabricated glass and t is the time period of dissolution. The behavior in Fig. 3 exhibited the increasing of durability with increasing of immersion time and decreased with increasing of Bi_2O_3 content. The increasing of *Dr* attributed to the hydration process resulted from the ion exchange in the glass network [29]. This hydration reduced noticeably by the increment of Bi_2O_3, which indicates that ability of bismuth oxide to improve water-resistant of the prepared glasses.

Shielding Properties

Table 1 shows density data, molar volume, packing density and other properties of the studied glass systems.

In the current study, we calculated the mass attenuation coefficients (μ/ρ) by using MCNP5 simulation code, Phy-X and XCOM software. Table 2 illustartes the calculated μ/ρ values of the new fabricated samples were estimated at six different energies (0.15, 0.5, 1, 3, 5 and 15 MeV). A good agreement between the performed methods as exhibited in Fig. 4. The new fabricated glasses showed decreasing in the calculated μ/ρ with increasing the energy of incident photon. Basically, the photoelectric effect is dominant at the low energy level (up to 0.1 MeV) due to the high effect of atomic number at this level (Z^{4-5}) [30, 31]. Thus, the μ/ρ values of the fabricated glass take the largest values in low energies then gradually decreased (Compton effect dominant) and finally, be almost constant at the level of 3–15 MeV due to the dominance of pair production (Z^2) [32, 33].

The buildup factor obtained from the contriution of scattering photon through exposure and absorption interaction. In the current study, we use the G–P fitting parameters to estimate both of exposure buildup factor (EBF) and energy absorption buildup factor (EABF) at different depths (1, 10, 20, 30 and 40 mfp).

The EBF for the S3 was estimated foe an incident photon in the energy levels of 0.01 to 15 MeV as shown in Figs. 5a, 5b. The EBF and EABF showed sharp peak at 0.9 MeV attributed to the *K*-absorption edge of

Table 1. The density (ρ) (g/cm^3), molar volume (V_m), Packing density (V_t), Poisson's ratio (σ), number of bonds per unit volume (N_B), metallization (M), average boron–boron separation $\times 10^{-23}$ $\langle d_{B-B} \rangle$ (Nm), molar polarizability $\times 10^{-24}$ (α_m) (cm)^3, refractive index (n) and dielectric constant (ε)

Code	ρ	V_m	V_t	σ	N_B	$\langle d_{B-B} \rangle$	α_m	n	ε	M
S1	4.244	18.122	0.909	0.347	9.969	1.433	4.058	2.211	4.888	0.435
S2	4.987	23.367	0.728	0.309	9.019	1.437	0.219	2.317	5.368	0.407
S3	5.732	27.246	0.644	0.284	8.178	1.371	0.264	2.388	5.702	0.389
S4	6.624	29.561	0.611	0.273	7.945	1.259	0.288	2.402	5.769	0.386

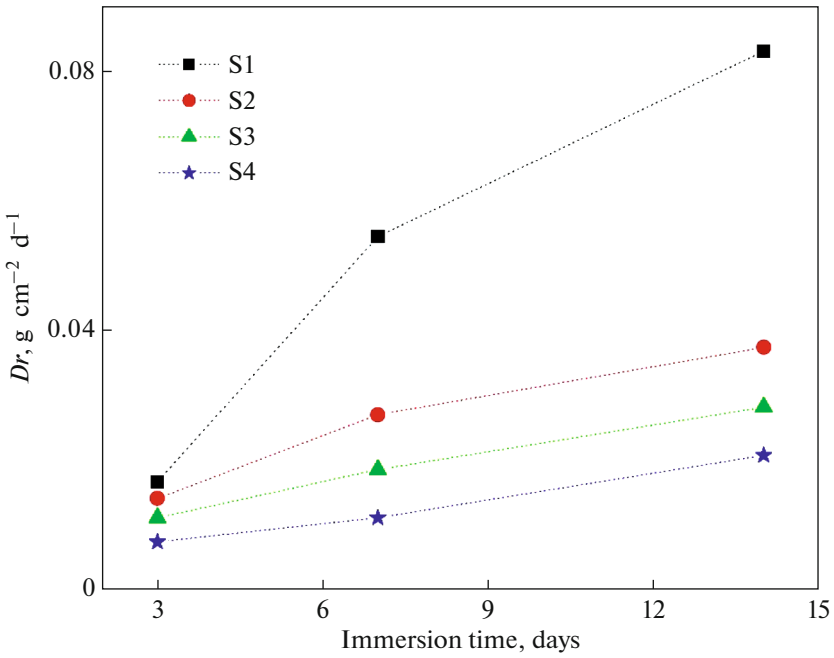

Fig. 3. Dissolution rates of the prepared glass for 14 days.

Bi [29]. Another small peak revealed at low energy level (0.3 MeV), which attributed to the *K*-shell absorption of Cd [34, 35]. The current spectra revealed that the values of exposure and absorption buildup factors are small at low levels (up to 0.1 MeV), then increased at the intermediate energy levels (0.1 up to1 MeV) and finaly decreased at high energy levels. The heightening of buildup factora at the intermediate level is attributed to the high likelihood of Compton scattering. Eventually the values decreased in high energy level due to pair production. Then start to increase again due to pair production process varies as $\sim Z^2$. In addi-

Table 2. Mass attenuation coefficients at specific energies (Phy-X, MCNP5 and XCOM)

	S1					S2				
	XCOM	Phy-X	Δ*a*	MCNP5	Δ*b*	XCOM	Phy-X	Δ*a*	MCNP5	Δ*b*
0.15	0.199	0.206	0.034	0.211	0.058	0.833	0.894	0.071	0.901	0.078
0.50	0.086	0.087	0.011	0.093	0.078	0.093	0.088	0.055	0.103	0.102
1.00	0.061	0.061	0.00	0.072	0.165	0.063	0.065	0.031	0.072	0.133
3.00	0.035	0.035	0.00	0.040	0.133	0.036	0.038	0.054	0.044	0.200
5.00	0.028	0.029	0.035	0.032	0.133	0.030	0.034	0.125	0.036	0.182
15.0	0.021	0.031	0.385	0.030	0.353	0.025	0.032	0.246	0.033	0.276
	S3					S4				
	XCOM	Phy-X	Δ*a*	MCNP5	Δ*b*	XCOM	Phy-X	Δ*a*	MCNP5	Δ*b*
0.15	1.335	1.323	0.001	1.348	0.010	1.836	1.818	0.010	1.822	0.010
0.50	0.100	0.110	0.095	0.116	0.148	0.108	0.115	0.063	0.122	0.121
1.00	0.063	0.067	0.061	0.071	0.119	0.064	0.069	0.075	0.088	0.315
3.00	0.037	0.039	0.052	0.043	0.150	0.037	0.040	0.078	0.042	0.126
5.00	0.031	0.037	0.176	0.039	0.228	0.033	0.038	0.141	0.041	0.216
15.0	0.028	0.034	0.193	0.039	0.328	0.032	0.040	0.222	0.047	0.379

$\Delta a = [(\text{XCOM-Phy-X})/((\text{XCOM} + \text{Phy-X})/2)] \times 100$.
$\Delta b = [(\text{XCOM-MCNP5})/((\text{XCOM} + \text{MCNP5})/2)] \times 100$.

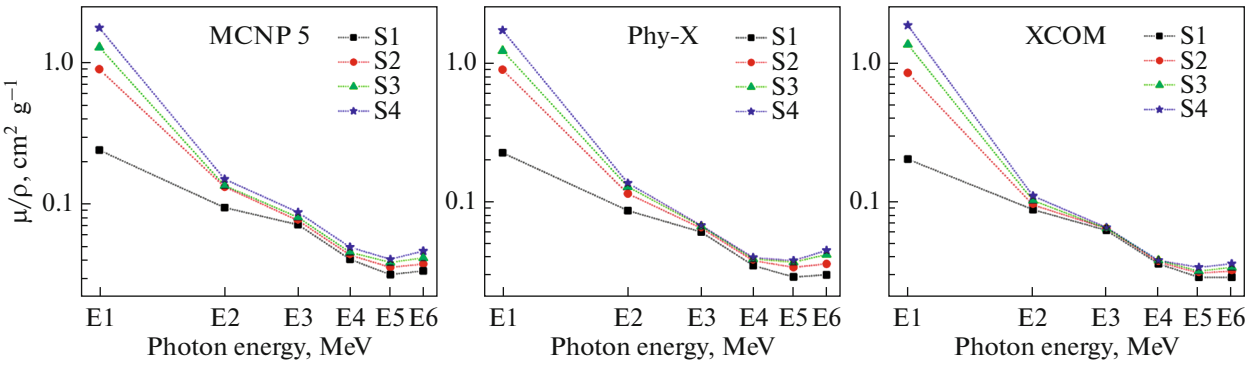

Fig. 4. The mass attenuation coefficients of the fabricated glasses using MCNP5, Phy-X and XCOM.

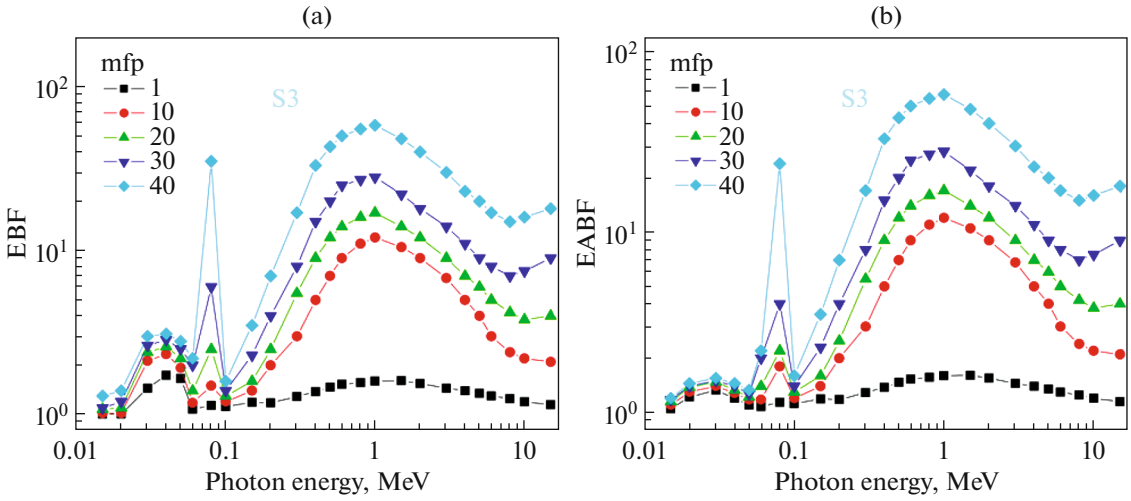

Fig. 5. The effect of energy on the (a) EBF and (b) EABF values for S3.

tion, the values of EBF and EABF clearly increased with increasing of penetration depths from one to 40 mfp.

Figure 6 shows the variation of the estimated electron densities for the prepared glasses at different energies (0.015, 0.05, 0.1, 0.5, 1, 5 and 15 MeV). The trend observe in the figure proved the depending of electron density on the incident of photon energy. For all glasses, the electron densities showed high values at low energy region (0.015, 0.05 and 0.1 MeV), and decreased at high energy region (0.5, 1, 5 and 15 MeV) [3]. In addition, it obvious the increasing of electron densities with the gradual increasing of Bi concentration.

The specific gamma-ray constant (aka gamma factor) is defined as the dose rate absorbed at a given material from a specific distance, and this factor used for radiation protection purposes to determine the dose collected at thickness or penetration depth in a specific material. Figure 7 illustrates the effect of different energy levels on the gamma factor for the new fabricated glasses. The values of specific gamma ray constant increase with increasing of incident photon energy [3, 34].

Figure 8 shows the dose rate variations (R/h) obtained from gamma ray energy with different thickness in a specific medium. The fabricated glasses were used as target or absorber for the incident energy. The dose rate variation was estimated at different thickness (0.1, 0.5, 1 and 1.5 cm). Furthermore, for all glasses and at different thickness the dose rate reduced at low energy level (0.015 up to 0.03 MeV), and then starting to increase from 0.04 up to 15 MeV.

It has already proved that neutron reactions increase with light element and decreases with increasing of neutron energy. In addition, the likelihood of neutron scattering increases gradually with the increase of collision occurred in the glass context. Consequently, it is important to examine the ability of neutron-energy retention through new shielding materials. For the current glasses, the effective removal cross-section for fast neutron (FRCS: Σ_R) was estimated mathematically and by using Ph-X program as shown in Table 3. Despite the reduction of neutron

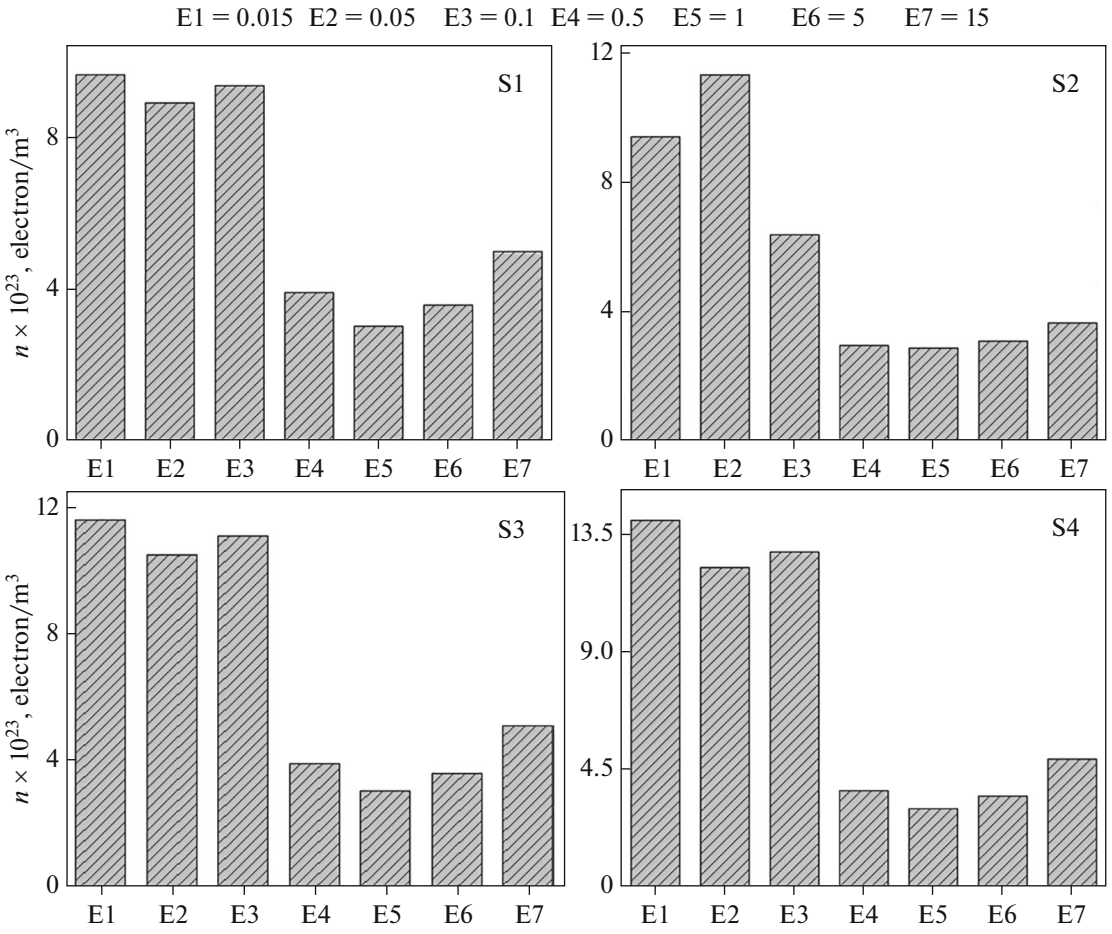

Fig. 6. The effective electron densities of the fabricated glasses at different energies.

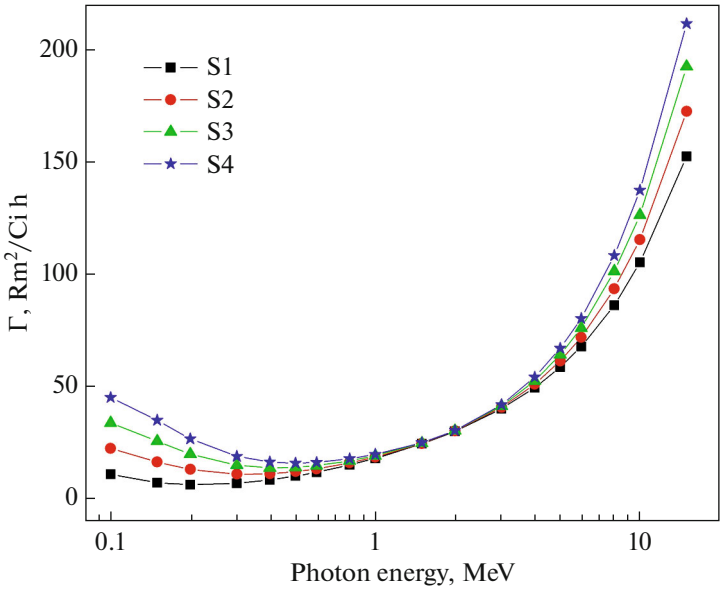

Fig. 7. The specific gamma ray constants for the fabricated glasses at different energy levels.

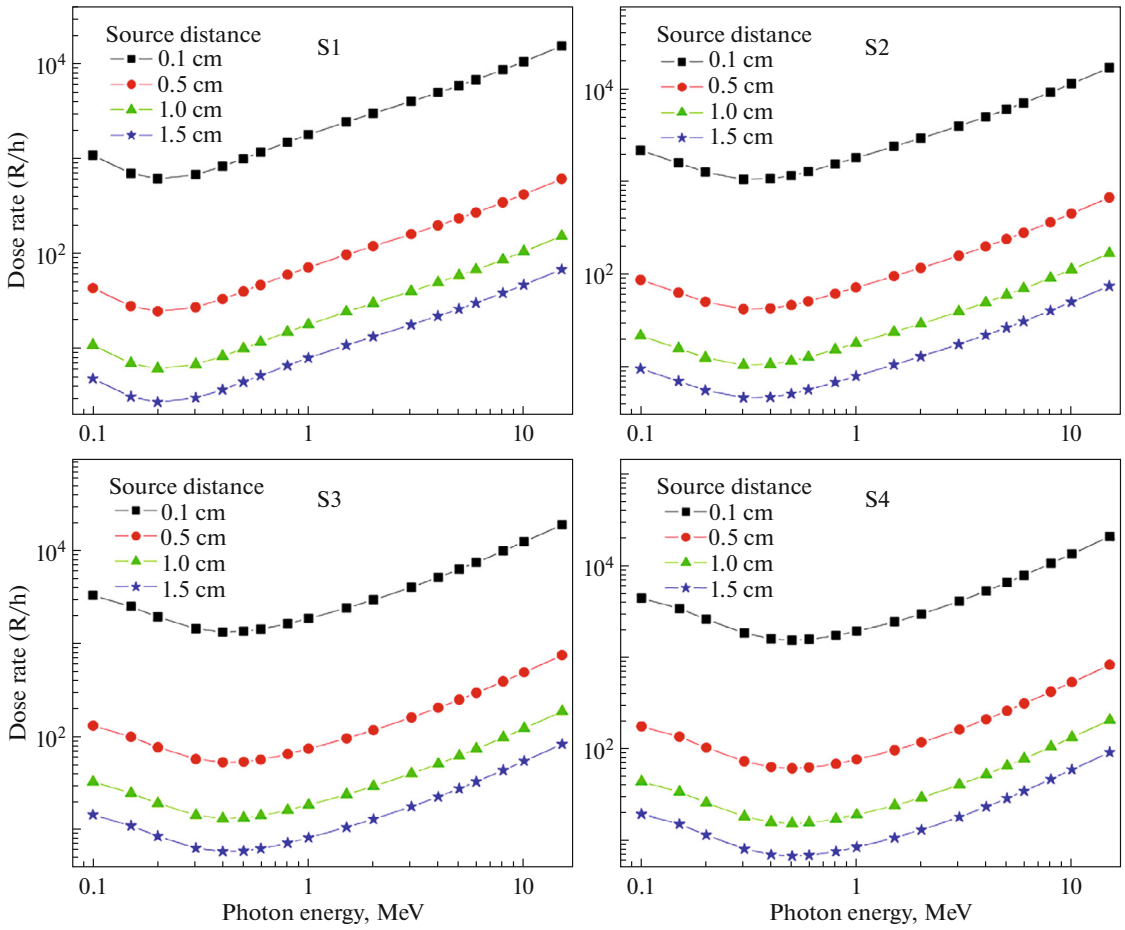

Fig. 8. The dose rate of gamma ray at different energies levels for the fabricated glasses.

Table 3. The removal cross-sections and mass removal cross-section for the fabricated glasses

Sample code	Element	Weight fraction	Partial density P, g cm^{-3}	Mass cross section Σ_R, cm^2 g^{-1}	Removal cross section Σ_R, cm^{-1}	
					manual calculation	using Phys-X
S1	B	0.1627	0.6906	0.0771	0.164	0.159
	O	0.4185	1.7759	0.0405		
	Na	0.1796	0.7621	0.0341		
	Cd	0.2392	1.0153	0.013		
S2	B	0.1010	0.5039	0.0771	0.141	0.137
	O	0.3057	1.5248	0.0405		
	Na	0.0719	0.3586	0.0341		
	Cd	0.1327	0.6617	0.013		
	Bi	0.3886	1.9381	0.0103		
S3	B	0.0621	0.3559	0.0771	0.132	0.129
	O	0.2316	1.3276	0.0405		
	Na	0.0569	0.3260	0.0341		
	Cd	0.1060	0.6074	0.013		
	Bi	0.5434	3.1150	0.0103		
S4	B	0.0386	0.2560	0.0771	0.131	0.128
	O	0.1879	1.2448	0.0405		
	Na	0.0470	0.3111	0.0341		
	Cd	0.0861	0.5704	0.013		
	Bi	0.6403	4.2417	0.0103		

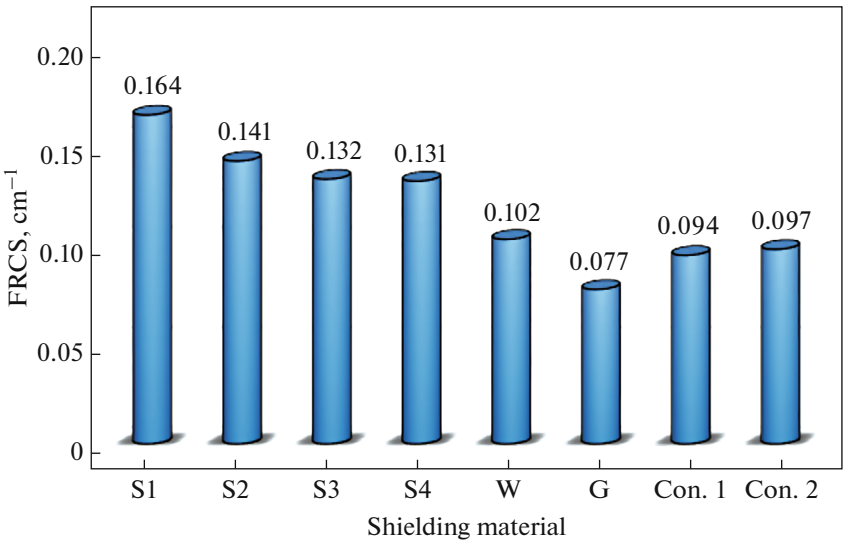

Fig. 9. The effective removal cross-section values of the fabricated glasses compared with other standard materials [W: water; G: graphite; Con. 1: ordinary concrete; Con. 2: serpentine concrete].

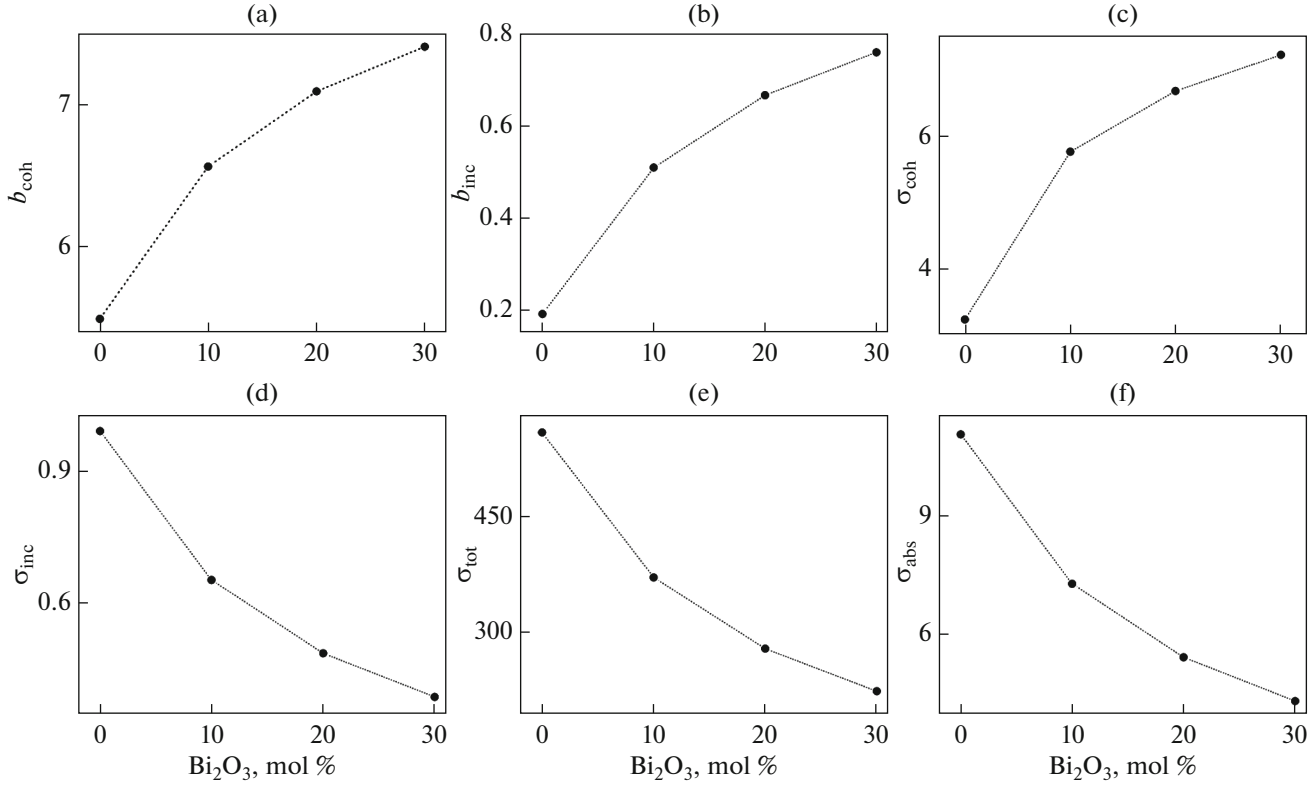

Fig. 10. The neutron scattering and absorption parameters for new prepared samples; (a) b_{coh}: the coherent neutron scattering length, (b) b_{inc}: the incoherent neutron scattering length, (c) σ_{coh}: the coherent neutron scattering cross section, (d) σ_{inc}: the incoherent neutron scattering cross section, (e) σ_{tot}: the total neutron scattering cross section, (f) σ_{abs}: the absorption neutron scattering cross section).

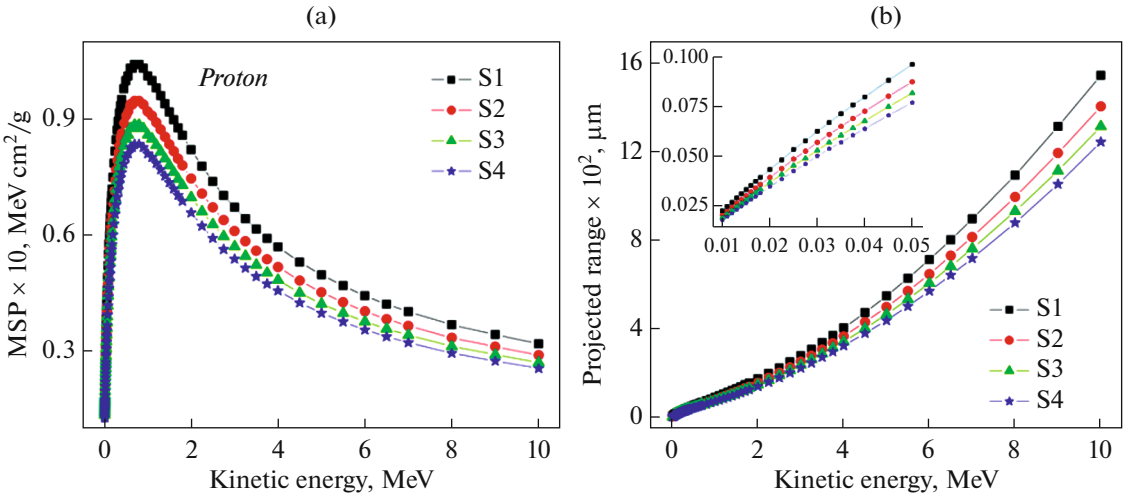

Fig. 11. Proton shielding properties for the prepared glasses as a function of kinetic energy for: a) mass stopping power variations; b) projected range variations.

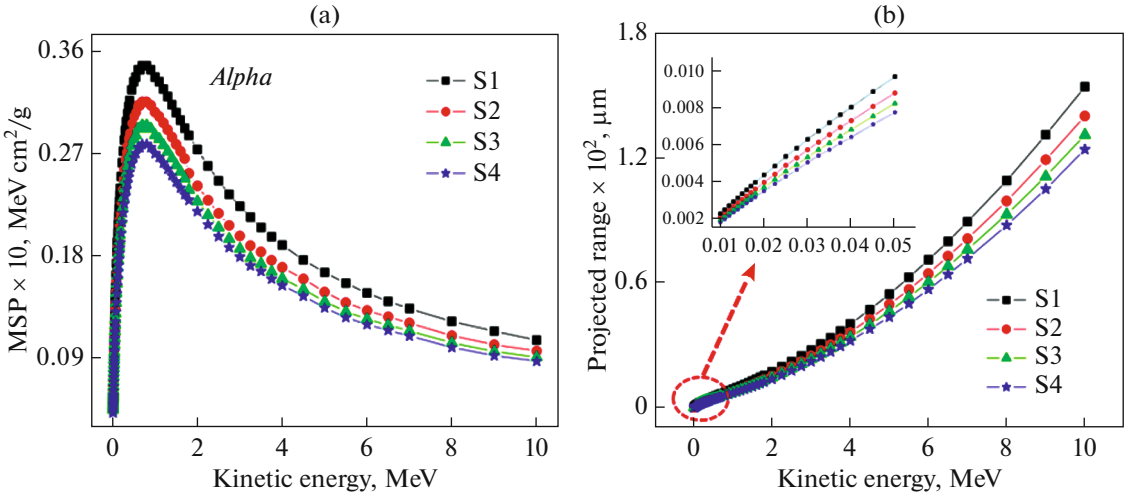

Fig. 12. Alpha shielding properties for the prepared glasses as a function of kinetic energy for: (a) mass stopping power variations; (b) projected range variations.

attenuation values reported with increasing Bi content, the Σ_R of all prepared glasses is better than some standard materials such as water (0.102 cm^{-1}), graphite (0.077 cm^{-1}) and concrete (ordinary = 0.094 cm^{-1} and serpentine = 0.097 cm^{-1}) as shown in Fig. 9 [36, 37].

Moreover, the neutron shielding parameters (NSP) for the new fabricated glassed were calculated concerning to the estimated mass fraction, neutron scattering lengths and cross sections of the elements of each single element in the glass compistion [38]. Six neutron scattering parameters (coherent and incoherent neutron scattering lengths, coherent and incoherent neutron scattering cross-sections, total and absorption neutron scattering cross-sections). Figure 10 reveled the growth of coherent/incoherent neutron scattering lengths and coherent neutron scattering cross-sections with increasing of Bi content. Conversely, the incoherent neutron scattering cross-sections, total and absorption neutron scattering cross-sections declined with increasing of Bi. The NSP attained by G4 are (b_{coh} = 7.40 fm; b_{inc} = 0.758 fm; σ_{coh} = 7.207 b and σ_{abs} = 4.352 b).

Figures 11 and 12 show the values of proton and alpha MSP of the prepared glasses. As shown in the figures, both values of proton and alpha increased with increasing of kinetic energy (up 1 MeV). In the energy range of 1 to 2 MeV, the MSP values radically decreased and the reduction continue in the higher energies (>2 MeV) but with low reduction rate. The sample with the highest Bi content (S4) revealed the lowest values of proton and alpha MSP.

The projected range is a concept that used to define the expected depth to which alpha or proton will penetrate up to rest in an absorber material [23]. In the current study, the projected ranges of proton and alpha were also determined by using SRIM code. A shown in Figs. 11 and 12, the prepared samples, especially S4, attained low projected range values.

CONCLUSION

Via the traditional melt-quench technique, four samples of $20Na_2O{\cdot}15CdO{\cdot}xBi_2O_3{\cdot}(65 - x)B_2O_3$ ($0.00 \le x \le 0.20$) were fabricated to assess their shielding features for different radiation types (photons, neutrons, alpha, and protons). The XRD instrument asserted the amorphous nature of the prepared samples. The replacement of Bi_2O_3 instead of B_2O_3 enhanced the density, durability, and μ/ρ values for the current samples, whereas the values of $\sum_R$, MSP and projected range for the alpha and protons display slightly decrement with addition Bi to the glass structure. Based on the obtained results, the current glass samples appear excellent shielding features for electromagnetic and particulate radiation nominate to utilize as structural shielding in different radiation facilities.

CONFLICT OF INTEREST

The authors declare than they have no conflict of interest.

REFERENCES

1. Obaid, S.S., Gaikwad, D.K., and Pawar, P.P., Determination of gamma ray shielding parameters of rocks and concrete, *Radiat. Phys. Chem.*, 2018, vol. 144, pp. 356–360.
2. Lukovic, J., Synthesis and characterization of tungsten carbide fine powder, *Ceram. Int.*, 2015, vol. 41, pp. 1271–1277.
3. Manjunatha, H.C., Seenappa, L., Chandrika, B.M., and Hanumantharayappa, C., A study of photon interaction parameters in barium compounds, *Ann. Nucl. Energy*, 2017, vol. 109, pp. 310–317.
4. Chang, Le., Zhang, Y., Yujian, L., Fang, J., Luan, W., Yang, X., Zhang, W., and Chang, L., Preparation and characterization of tungsten/epoxy composites for γ-ray radiation shielding, *Nucl. Instrum. Methods Phys Res., Sect. B*, 2015, vol. 356, pp. 88–93.
5. Ogawa, M., Two cased of acute lead poisoning due to occupational exposure to lead, *Clin. Toxical.*, 2015, vol. 46, pp. 332–335.
6. Zuguchi, M., Usefulness of non-lead aprons in radiation protection for phusicians performing international procedure, *Radiat. Prot. Dosim.*, 2008, vol. 131, pp. 531–534.
7. Singh, M., Tondon, A., Sandhu, B.S., and Singh, B., Energy dependence of radiation interaction parameters of some organic compounds, *Radiat. Phys. Chem.*, 2018, vol. 145, pp. 80–88.
8. Demayo, A., Taylor, M.C., Taylor, K.W., Hodson, P.V., and Hammond, P.B., Toxic effects of lead and lead compounds on human health, aquatic life, wildlife plants, and livestock, *Crit. Rev. Environ. Control*, 1982, vol. 12, pp. 257–305.
9. Pomaro, B., A review on radiation damage in concrete for nuclear facilities: From experiments to modeling, *Model. Simul. Eng.*, 2016, vol. 2016, pp. 1–10.
10. Ozdemira, T., Gungora, A., Akbaya, K., Uzuna, H., and Babuccuoglub, Y., Nano lead oxide and EPDM composite for development of polymer based radiation shielding material: Gamma irradiation and attenuation tests, *Radiat. Phys. Chem.*, 2018, vol. 144, pp. 248–255.
11. Kumar, A., Gamma ray shielding properties of PbO-Li_2O-B_2O_3 glasses, *Radiat. Phys. Chem.*, 2017, vol. 136, pp. 50–53.
12. Gaik, M., Elbashir, B.O., and Sayyed, M.I., Enhancement of gamma ray shielding properties by PbO partial replacement of WO_3 in ternary $60TeO_2$–$(40 - x)WO_{3-x}$PbO glass system, *Chalcogenite Lett.*, 2017, vol. 14, pp. 113–118.
13. Gaikwad, D.K., Sayyed, M.I., Obaid, S.S., Issa, S.A.M., and Pawar, P.P., Gamma ray shielding properties of TeO_2–ZnF_2–As_2O_3–Sm_2O_3 glasses, *J. Alloys Compd.*, 2018, vol. 765, pp. 451–458.
14. Zoulfakar, A.M., Abdel-Ghany, A.M., Abou-Elnasr, T.Z., Mostafa, A.G., Salem, S.M., and El-Bahnaswy, H.H., Effect of antimony-oxide on the shielding properties of some sodium-boro-silicate glasses, *Appl. Radiat. Isotopes*, 2017, vol. 27, pp. 269–274.
15. Kaur, P., Singh, K.J., Thakur, S., Singh, P., and Bajwa, B.S., Investigation of bismuth borate glass system modified with barium for structural and gamma-ray shielding properties, *Spectrochim. Acta, Part A*, 2019, vol. 206, pp. 367–377.
16. Gao, G., Hu, L., Fan, H., Wang, G., Li, K., Feng, S., Fan, S., and Chen, H., Effect of Bi_2O_3 on physical, optical and structural properties of boron silicon bismuthate glasses, *Opt. Mater.*, 2009, vol. 32, pp. 159–163.
17. El Batal, F.H., Gamma ray interaction with bismuth silicate glasses, *Nucl. Instrum. Methods Phys. Res., Sect. B*, 2007, vol. 254, pp. 243–253.
18. El Batal, F.H., Marzouk, M.A., and Abdelghany, A.M., Gamma rays interaction with bismuth borate glasses doped by transition metal ions, *J. Mater. Sci.*, 2011, vol. 46, pp. 5140–5152.
19. Gomaa, M.M., Ibrahim, S., and Darwish, H., Effect of SiO_2/B_2O_3 replacements on the structure, physicochemical and electrical properties of Bi_2O_3-containing glasses, *Silicon*, 2015, vol. 7, pp. 55–63.
20. Ou, Y., Baccaro, S., Zhang, Y., Yang, Y., and Chen, G., Effect of gamma-ray irradiation on the optical properties of PbO–B_2O_3–SiO_2 and Bi_2O_3–B_2O_3–SiO_2 glasses, *J. Am. Ceram. Soc.*, 2010, vol. 93, pp. 338–341.
21. Sharma, G., Thind, K.S., Singh, Monika., Manupriya, H., and Gerward, L., Optical properties of heavy metal oxide glasses before and after gamma-irradiation, *Phys. Status Solidi A*, 2007, vol. 204, pp. 591–601.
22. Sakar, E., Firat, O., Alim, B., Sayyed, M.I., and Kurudirek, M., Phys-X/PSD: Development of a user friendly online software for calculation of parameters relevant

to radiation shielding and dosimetry, *Radiat. Phys. Chem.*, 2020, vol. 166, 108496.

23. Ziegler, J.F., Biersack, J.P., and Ziegler, M.D., *SRIM—The Stooping Range of Ions in Matter*, SRIM, 2008.
24. The Stopping and Range of Ions in Matter (SRIM). www.srim.org.
25. Dong, M.G., El-Mallawany, R., Sayyed, M.I., and Tekin, H.O., Shielding properties of $80TeO_2$–$5TiO_2$–$(15-x)WO_{3-x}$AnOm glasses using WinXcom and MCNP5 code, *Radiat. Phys. Chem.*, 2017, vol. 141, pp. 172–178.
26. Tekin, H.O. and Kara, U., Monte Carlo simulation for distance and absorbed dose calculations in a PET-CT facility by using MCNP-X, *J. Commun. Comput.*, 2016, vol. 13, pp. 32–35.
27. Mahmoud, K.A., Sayyed, M.I., and Tashlykov, O.L., Comparative studies between the shielding parameters of concretes with different additive aggregates using MCNP-5 simulation code, *Radiat. Phys. Chem.*, 2019, vol. 165, 108426.
28. Koudelka, L., Kalenda, P., Mosner, P., Montagne, L., and Revel, B., Structure and properties of barium niobophosphate glasses, *J. Non-Cryst. Solids*, 2019, vol. 459, pp. 68–74.
29. Parminder Kaur, Singh, K.J., Kurudirek, M., and Thakur, S., Study of environment friendly bismuth incorporated lithium borate glass system for structural, gamma-ray and fast neutron shielding properties, *Spectrochim. Acta*, *Part A*, 2019, vol. 223, 117309.
30. Dong, M.G., Sayyed, M.I., and Lakshminarayana, G., Çelikbilek Ersundu, M., Priyanka Nayar, A.E., and Mahdi, M.A., Investigation of gamma radiation shielding properties of lithium zinc bismuth borate glasses using XCOM program and MCNP5 code, *J. Non-Cryst. Solids*, 2017, vol. 468, pp. 12–16.
31. Parandamaiah, M., Kumar, K.N., Babu, S., Reddy, S.V.R., and Ratnakaram, Y.C., Dy^{3+} doped lithium sodium bismuth borate glasses for yellow luminescent photonic applications, *Int. J. Eng. Res. Appl.*, 2015, vol. 5, pp. 126–131.
32. Olarinoye, I.O., Odiaga, R.I., and Paul, S., EXABCal: A program for calculating photon exposure and energy absorption buildup factors, *Heliyon*, 2019, vol. 5, e02017.
33. Mhareb, M.H.A., Almessiere, M.A., Sayyed, M.I., and Alajerami, Y.S.M., Physical, structural, optical and photons attenuation attributes of lithium–magnesium–borate glasses: Role of Tm_2O_3 doping, *Optik*, 2019, vol. 182, pp. 821–831.
34. Alajerami, Y.S., Drabold, D., Mhareb, M., and Katherine Leslee, A., Cimatu, G.Ch., and Kurudirek, M., Radiation shielding properties of bismuth borate glasses doped with different concentrations of cadmium oxides, *Ceram. Int.*, 2020, vol. 46, no. 8, pp. 12718–12726.
35. Saddeek, Y.B., Issa, Sh.A.M., Alharbi, T., Aly, K., Ahmad, M., and Tekin, H.O., Mechanical and nuclear shielding properties of sodium cadmium borate glasses: Impact of cadmium oxide additive, *Ceram. Int.*, 2020, vol. 46, no. 3, pp. 2661–2669.
36. Singh, V.P. and Badiger, N., Shielding efficiency of lead borate and nickel borate glasses for gamma rays and neutrons, *Glass Phys. Chem.*, 2015, vol. 42, no. 3, pp. 276–283.
37. El Abd, A., Mesbah, G., Nader Mohamed, M.A., and Ellithi, A., A simple method for determining the effective removal cross section for fast neutrons, *J. Radiat. Nucl. Appl.*, 2017, vol. 2, no. 2, pp. 53–58.
38. Sears, V.F., Neutron scattering lengths and cross section, *Neutron News*, 1992, vol. 3, no. 3, pp. 26–37.